DOT/FAA/NR-92/8, II

Program Director for Surveillance
Washington, DC 20591

(2)

On the Potential Use of the Terminal Doppler Weather Radar Gust Front Detection Algorithm On the WSR-88D System

Part II: Detecting Non-Gust Front Convergent Weather Phenomena

Gregory J. Stumpf

NOAA/ERL National Severe Storms Laboratory
1313 Halley Circle
Norman, OK 73069

and

Cooperative Institute for Mesoscale Meteorological Studies
University of Oklahoma
Norman, OK 73019

October 1991

"Original contains color plates: All DTIC reproductions will be in black and white"

Interim Report

U.S. Department of Transportation
Federal Aviation Administration

DISCLAIMER NOTICE

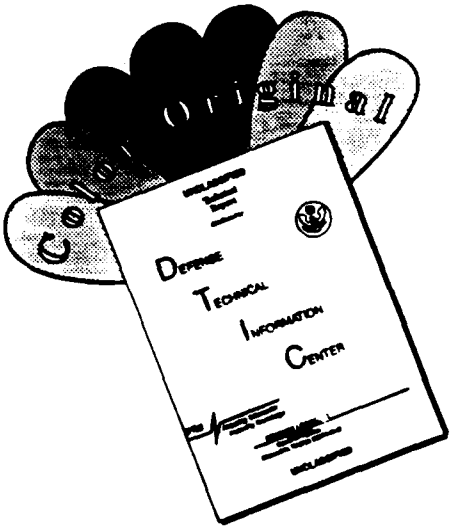

THIS DOCUMENT IS BEST QUALITY AVAILABLE. THE COPY FURNISHED TO DTIC CONTAINED A SIGNIFICANT NUMBER OF COLOR PAGES WHICH DO NOT REPRODUCE LEGIBLY ON BLACK AND WHITE MICROFICHE.

Technical Report Documentation Page

1. Report No.	2. Government Accession No.	3. Recipient's Catalog No.
DOT/FAA/NR-92/8, II		

4. Title and Subtitle

On the Potential Use of the Terminal Doppler Weather Radar Gust Front Detection Algorithm on the WSR-88D System
Part II: Detecting Non-gust Front Convergent Weather Phenomena

5. Report Date
October 1991

6. Performing Organization Code

8. Performing Organization Report No.

7. Author(s)
Gregory J. Stumpf

9. Performing Organization Name and Address

NOAA/ERL National Severe Storms Laboratory
1313 Halley Circle
Norman, OK 73069

10. Work Unit No. (TRAIS)

11. Contract or Grant No.
DTFAO1-80-Y-10524

13. Type of Report and Period Covered
Interim Report

12. Sponsoring Agency Name and Address

U.S. Department of Transportation
Federal Aviation Administration
800 Independence Avenue, SW
Washington, DC 20591

14. Sponsoring Agency Code
ANR-150

15. Supplementary Notes

16. Abstract

This study examines the capability of the Gust Front Detection Algorithm (GFDA) developed for the Terminal Doppler Weather Radar (TDWR) system to detect other types of non-gust front weather phenomena which are associated with patterns of convergence in a Doppler-radar radial velocity field. The potential use of the GFDA as a nowcasting tool, a mesoscale forecasting tool, and as a tool to detect other kinds of aviation hazards besides gust fronts, needs investigation. The phenomena studied include synoptic fronts, sea-breeze fronts, gravity waves, terrain-induced convergence boundaries, old thunderstorm outflow boundaries, and the convergence bands within extratropical cyclones associated with enhanced precipitation. Comparisons of the convergent characteristics of these other phenomena to those of gust fronts are made. In addition, several case studies are presented to demonstrate the ability of the GFDA to detect the non-gust front phenomena.

17. Key Words	18. Distribution Statement
Doppler Radar, Algorithm, Aviation, Gust Front, Wind Shift, WSR-88D, TDWR, NWS, AWS	This document is available to the public through the National Technical Information Service, Springfield, VA 22161.

19. Security Classif. (of this report)	20. Security Classif. (of this page)	21. No. of Pages	22. Price
Unclassified	Unclassified	43	

Form DOT F 1700.7 (8-72) Reproduction of completed page authorized

ACKNOWLEDGMENTS

The author thanks Mike Eilts, Laurie Hermes, Diana Klingle-Wilson, Don Burgess, Dr. Dusan Zrnić, Kevin Thomas, Matt Gilmore, DeWayne Mitchell, Mike Jain, and Dr. Edward Brandes for their assistance and valuable comments. Doppler radar data were provided by the MIT Lincoln Laboratory under sponsorship from the Federal Aviation Administration. Radar data were also furnished by the National Severe Storms Laboratory.

TABLE OF CONTENTS

LIST OF FIGURES

LIST OF TABLES

ACRONYMS

DCVZ	Denver Convergence Vorticity Zone
FL-2	10-cm Doppler radar operated by MIT/LL
GFDA	Gust Front Detection Algorithm
LL	Lincoln Laboratory
MIT	Massachusetts Institute of Technology
NSSL	National Severe Storms Laboratory
OT&E	Operational Test and Evaluation
SNR	Signal-to-noise ratio
TDWR	Terminal Doppler Weather Radar
UTC	Coordinated Universal Time
UWA	Uniform Wind Analysis
WSR-88D	Next Generation Weather Radar (formerly NEXRAD)

1. Introduction.

The Terminal Doppler Weather Radar (TDWR) Gust Front Detection Algorithm (GFDA) has been developed to detect and forecast gust fronts that produce wind shear hazards and significant wind shifts that affect airport operations. The GFDA relies on pattern recognition in Doppler-radar radial velocity fields to determine gust front locations. A gust front will typically appear as a semi-linear region of decreasing radial velocities that identify radial convergence. Several constraints are used in the algorithm to maximize the probability of detecting gust fronts, yet at the same time, keeping the number of false detections low. These constraints include minimum length and strength thresholds, and vertical continuity constraints (i.e., convergence must be found on more than one low-altitude tilt of Doppler radar data from the same scan time). Selection of these site-adaptable threshold parameters (Witt et al., 1989) constrains the GFDA to identify those radial convergent patterns matching the characteristics of gust fronts.

Since the TDWR GFDA may be transferred to the WSR-88D system in the future, there is the potential to use the GFDA for other purposes besides detecting gust fronts in the terminal environment of commercial airports. For example, the United States Air Force Air Weather Service (AWS), a future user of the WSR-88D, could use the GFDA as an aircraft hazard warning tool at military airports. The FAA will be using the WSR-88D for enroute aircraft operations. And finally, the National Weather Service (NWS) could use the GFDA as a tool for detecting the

radial convergence patterns associated with not only gust fronts, but with other forms of weather phenomena characterized by convergent wind fields. Detection of such phenomena may provide the NWS meteorologist information for the mesoscale forecasts of convective initiation, precipitation amounts, and events producing severe wind gusts. [Part I of this study addresses the impacts of the radar system differences between the TDWR and WSR-88D on the performance of the algorithm (Stumpf, 1991)].

The potential use of the GFDA as a nowcasting tool, a mesoscale forecasting tool, and as a tool to detect other kinds of aviation hazards besides gust fronts, needs investigation. Therefore, this study has been conducted to examine the potential use of the GFDA to detect different kinds of weather phenomena associated with convergent wind fields. These include: 1) synoptic cold fronts and gravity waves that have been shown to be potentially hazardous to aviation [Browning (1971), Christie and Muirhead (1983), respectively], 2) sea/lake/land breeze fronts, orographically-induced boundary-layer convergence lines, "mountain outflows", and old thunderstorm outflow boundaries that have been identified as convection precursors [Wilson and Schreiber (1986), Szoke *et al.* (1984), Schlatter (1985), Purdom (1982), respectively]; and 3) the convergence bands within extratropical cyclones associated with mesoscale areas of enhanced precipitation (Ramamurthy *et al.*, 1991). Comparisons of the convergent characteristics of these other phenomena to those of gust fronts will be made. In addition, several case studies are presented to demonstrate the ability of the GFDA to detect the non-gust front phenomena.

2. The Gust Front Detection Algorithm.

2.1 Background.

The initial development of the GFDA began in the early 1980's at the National Severe Storms Laboratory (NSSL; Uyeda and Zrnić, 1985). Since then, several upgrades to algorithm techniques have been made (Witt and Smith, 1987; Witt et al., 1989; Hermes et al., 1990).

The algorithm relies on identifying the main attribute which gust fronts possess in Doppler-radar radial velocity fields, i.e., lines of radial convergence. An Advanced Gust Front Detection Algorithm (AGFDA; Eilts et al., 1991), currently under development, uses azimuthal shear and reflectivity thin line recognition capability to improve gust front detectability. This report focuses on only the radial convergence algorithm, the GFDA. Section 2.2 will briefly describe the techniques used to detect the radial convergent portion of gust fronts. The reader is asked to refer to Witt et al. (1989) for a more comprehensive description of the GFDA.

2.2 Gust front detection techniques.

The GFDA uses velocity data from two low-altitude elevation scans (0.5° and 1.0°). The algorithm builds radially convergent *shear segments* from smoothed and

dealiased velocity data. These shear segments consist of runs of decreasing radial velocity. As each shear segment is built, several attributes of the segment are compared to minimum thresholds. Thresholded are the *velocity difference* between the beginning and ending velocities of the segment (Δv), and the maximum velocity difference computed over a ≈1 km distance within the segment (called *peak shear*). Typical threshold settings (used during real-time testing at Denver Colorado in 1988) are $\Delta v = 7$ m s^{-1} for the 0.5° tilt, $\Delta v = 5$ m s^{-1} for the 1.0° tilt, and peak shear = 2 m s^{-1} km^{-1} for both tilt angles. These thresholds have been chosen empirically to increase probability of gust front detection while reducing the number of false alarms. The *peak shear location* is defined by the slant range to the center of the 1 km window over which the peak shear is calculated.

Individual shear segments are combined into *shear features* based on spatial proximity. Shear segments are placed into a common feature if their peak shear locations are separated by no more than 2.2° in azimuth and 2 km in range. If there are fewer than five segments in the feature, that feature is discarded. Two features from the same elevation scan are combined if the end points of the features are within 5 km of each other. Shear features from the two low-altitude scans are *vertically associated* to declare *gust front detections*, and the peak shear locations are represented as a smooth curve.

If one or more gust fronts are detected on two consecutive radar volume scans, an attempt is made to establish time continuity between fronts. If a front has been time associated, 10 and 20 minute forecast positions are produced by the

algorithm, and an attempt is made to estimate the horizontal wind speed and direction on both sides of the gust front. Finally, an estimate of the wind shear that an aircraft might experience upon encountering a gust front (wind shear hazard) is computed. This estimate is the sum of the mean plus one standard deviation of every peak shear values for each shear feature used in making a gust front detection.

3. Data.

A limited set of radar data was available to use as case studies. These data consisted of Doppler-radar radial velocity data collected at low-altitude tilt angles. The data were collected at sites in Central Oklahoma by the National Severe Storms Laboratory (NSSL) 10-cm Norman Doppler radar, and near Denver, Colorado, and near Orlando, Florida, by the Massachusetts Institute of Technology Lincoln Laboratory (MIT/LL) FL-2 testbed radar. Archive data from 1987, 1988, and 1990 were used.

The GFDA is designed to run with a TDWR tilt sequence using two low-altitude tilts, namely 0.5° and 1.0°. Most of the Norman data were collected using a different tilt sequence that did not include these two tilt angles, so the two tilts closest to 0.5° and 1.0° were used.

4. Methodology.

The version of the TDWR GFDA developed in 1989 (Hermes et al., 1990) was used to analyze the case study data. This version of the algorithm was used to take advantage of its improved vertical association and feature separation procedures. A listing of some of the site-adaptable parameters used for the analyses is shown in Table 1. The testing was carried out using the default parameter settings used during the 1988 TDWR OT&E (Operational Test and Evaluation) in Denver Colorado to simulate detecting actual gust fronts. A list of the definitions of these parameters and suggested values are summarized in Appendix B of Witt et al. (1989).

Table 1. Algorithm site-adaptable attribute settings used for the test runs.

PARAMETER	VALUE
Lower Tilt Angle	0.5°
Upper Tilt Angle	1.0°
Minimum Processing Range	3.0 km
Maximum Processing Range	60.0 km
Signal-to-noise Threshold	0
Velocity Difference Threshold Lower Tilt	7.0 m/s
Velocity Difference Threshold Upper Tilt	5.0 m/s
Peak Shear Threshold Lower Tilt	2.0 m/s/km
Peak Shear Threshold Upper Tilt	2.0 m/s/km
Minimum Radial Spacing	2.0 km
Minimum Azimuthal Spacing	2.2°
Minimum Number of Segments for Feature	5
Feature Connection Threshold	5.0 km
Minimum Single Feature Length	5.0 km
Minimum Combined Feature Length	5.0 km
Minimum Length of Front	10.0 km
Vertical Correlation Distance	2.0 km

The values in Table 1 have been chosen to most closely match the characteristics of gust fronts. The Velocity Difference and Peak Shear thresholds basically

define the strength of the gust front. The Minimum Radial Spacing, Minimum Azimuthal Spacing, and the Feature Connection thresholds constrain these patterns of radial convergence to a semi-linear shape. The Minimum Number of Segments, and the three length thresholds, constrain the length of gust fronts to at least 10 km. Finally, the Vertical Correlation Distance is set such that proper vertical association of shear features from both tilts is made.

5. Detecting non-gust front convergent weather phenomena.

5.1 Synoptic cold fronts.

The conceptual model of a synoptic cold front is comparable to a gust front; both are convergent phenomena with a semi-linear shape, have depths around 1-2 km, and are leading edges of cold air masses. Although cold fronts resemble gust fronts, their origin is not of a convective nature, nor do they have a convective-scale extent. Instead, they represent the boundary between two distinctly different synoptic-scale air masses (Parsons, 1991). Because cold fronts are synoptic-scale phenomena, their length will be greater the typical length of gust fronts.

Since the wind shears across cold fronts can be comparable to gust fronts, they can also be a threat to aviation. The knowledge of an approaching wind shift associated with any strength of synoptic cold front would be useful for runway management. Similar to gust fronts, synoptic cold fronts vary in propagation speed, width, length, depth, precipitation type and amount, and temperature, humidity, and

velocity differences. Also, these characteristics are seasonally and regionally dependent.

Detecting non-precipitating cold fronts will pose the greatest problem. To detect most non-precipitating fronts, a radar must have sufficient "clear-air" sensitivity (Brandes and Rabin, 1991), such as the TDWR and WSR-88D radars. Similar to many gust fronts, these precipitation-free synoptic fronts suffer from weak radar echo return. Echo return in precipitation-free environments is usually caused by variations in atmospheric refractive indexes due to enhanced gradients of moisture and temperature (Doviak and Zrnić, 1984). As colder air moves over warm surfaces, there is turbulence and mixing, and the refractive indexes increase. However, precipitation-free fronts have been observed to raise debris off the ground [such as insects, seeds, or wheat chaff (Wilson and Schreiber, 1986)]) which can also augment reflectivity. The contribution of refractive index gradients to reflectivity will vary seasonally as humidities are generally lower in wintertime environments. The contribution of windswept debris to reflectivity will depend on the dryness and looseness of soil over which fronts will pass. This is a factor of season, vegetation and soil types, and geographic location.

Browning (1971) used a Doppler radar to study the cross-sectional airflow across a cold front (Fig. 1). The low-altitude velocity difference across the leading edge of this cold front was measured at 14 m s^{-1} over a 500 m distance. Since this velocity difference was well above the suggested algorithm threshold value for minimum velocity difference (7 m s^{-1}), this front should be detected. The depth of

the converging velocities is about 1 km, within the range of typical gust front depths (Klingle *et al.*, 1987).

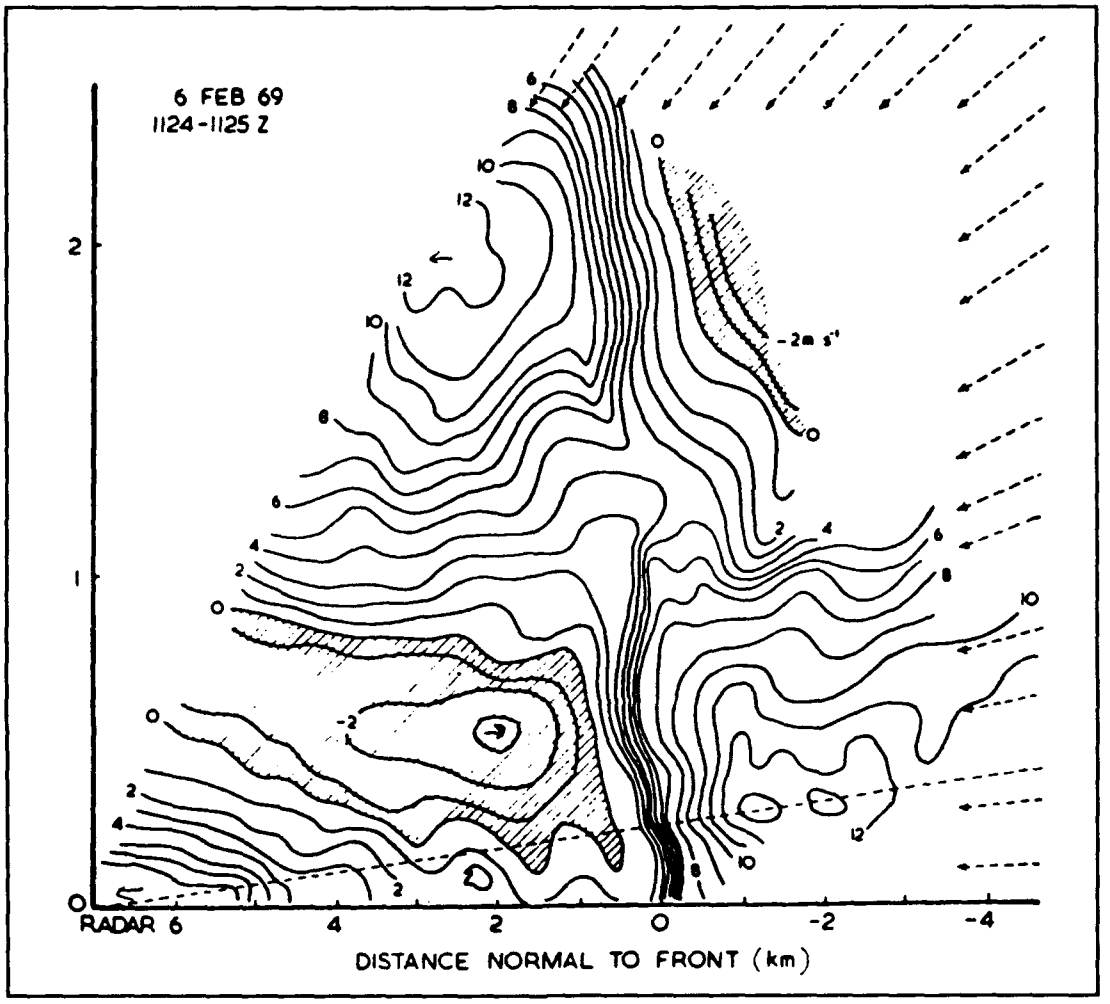

Fig. 1. Doppler radar wind component across a cold front on 6 February 1969. Front is moving to the right. Isotachs are at intervals of 1 m s^{-1}. Hatched shading indicates outbound velocities. From Browning (1971).

The GFDA should be able to detect any synoptic cold front that has a velocity difference >7 m s^{-1} over at a continuous 10-km length as long as there is enough returned echo on either side of the front. Shallow and distant synoptic cold fronts will be difficult to detect at far ranges. Of course, detectability will be different for every cold front since convergence strength and depth will vary from front to front.

The GFDA was tested using Doppler radar data from a synoptic cold front which passed through Oklahoma on 24 March 1988. A large portion of the cold front which crossed the Norman radar was unaccompanied by precipitation. When the front was northwest of the radar (1949 UTC), it consisted of 2 parallel, narrow lines or bands of signal return each about 5-7 km wide, and each about 25 km apart (Fig. 2; discussion of the double line structure of this front is beyond the scope of this study, and the front will be defined as the band closer to the radar). Only weak convergence was obvious along that portion of the front which was oriented normal to the radar radials. Signal was weak throughout most of the domain and detections were hampered. The algorithm detected only one 10-km shear feature on the 1.0° tilt.

The front passed the radar by 2155 UTC. A detection was produced along a 60 km length of the front (Fig. 3). In the vicinity of the front, much more signal was being returned to the radar than at earlier times. Velocity differences across the gust front detection averaged about 12 m s^{-1} and were as high as 19 m s^{-1} (well above the threshold setting of 7 m s^{-1}). A reflectivity thin line, with average maximum reflectivities of 20 dBZ, was also observed.

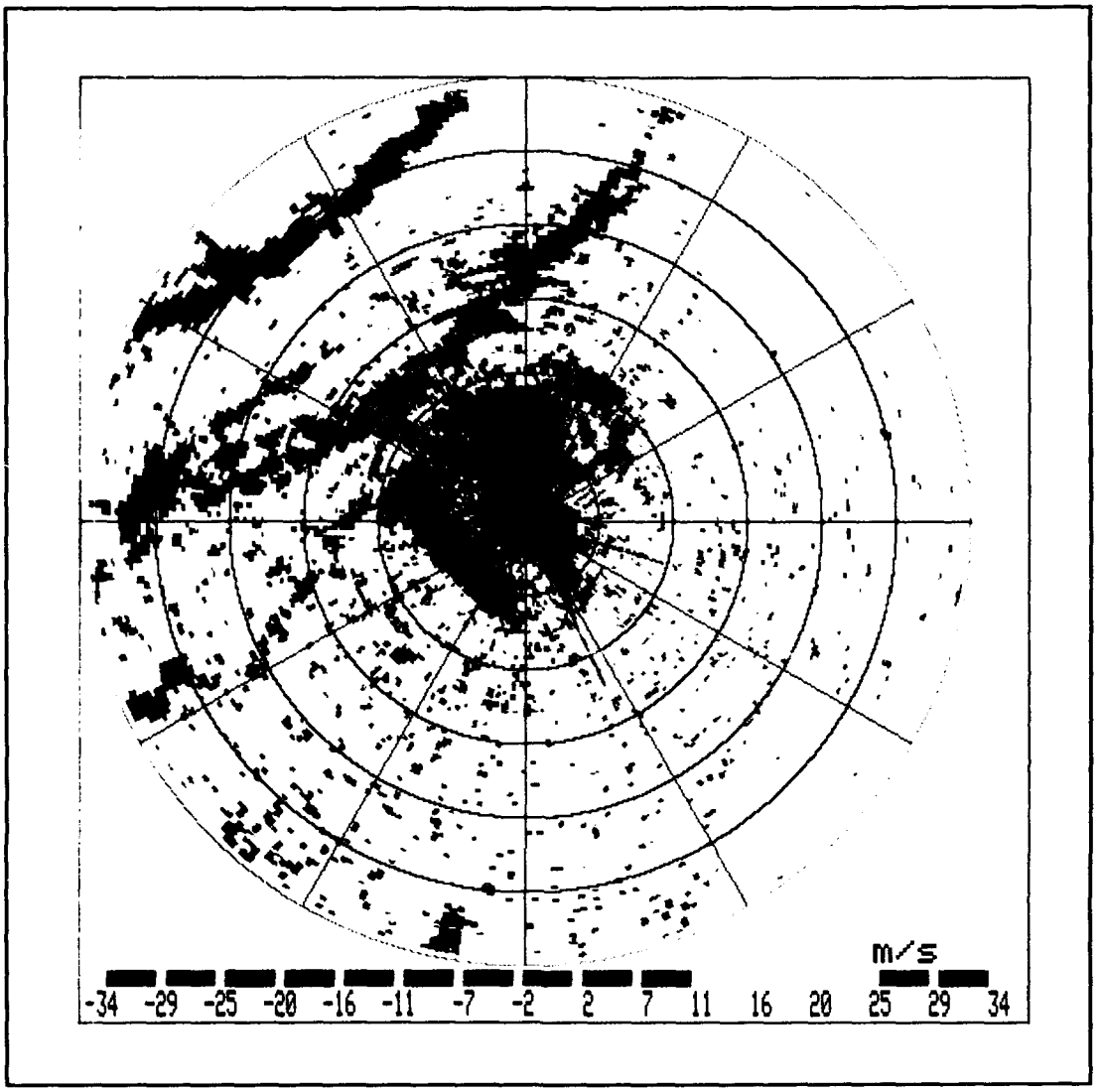

Fig. 2. Radial velocity field for the 1.0° tilt at 1949 UTC 24 March 1988 from the National Severe Storms Laboratory (NSSL) Norman, Oklahoma Doppler radar. Range rings are every 10 km. Positive (negative) velocity values (m s^{-1}) represent velocities away (toward) the radar.

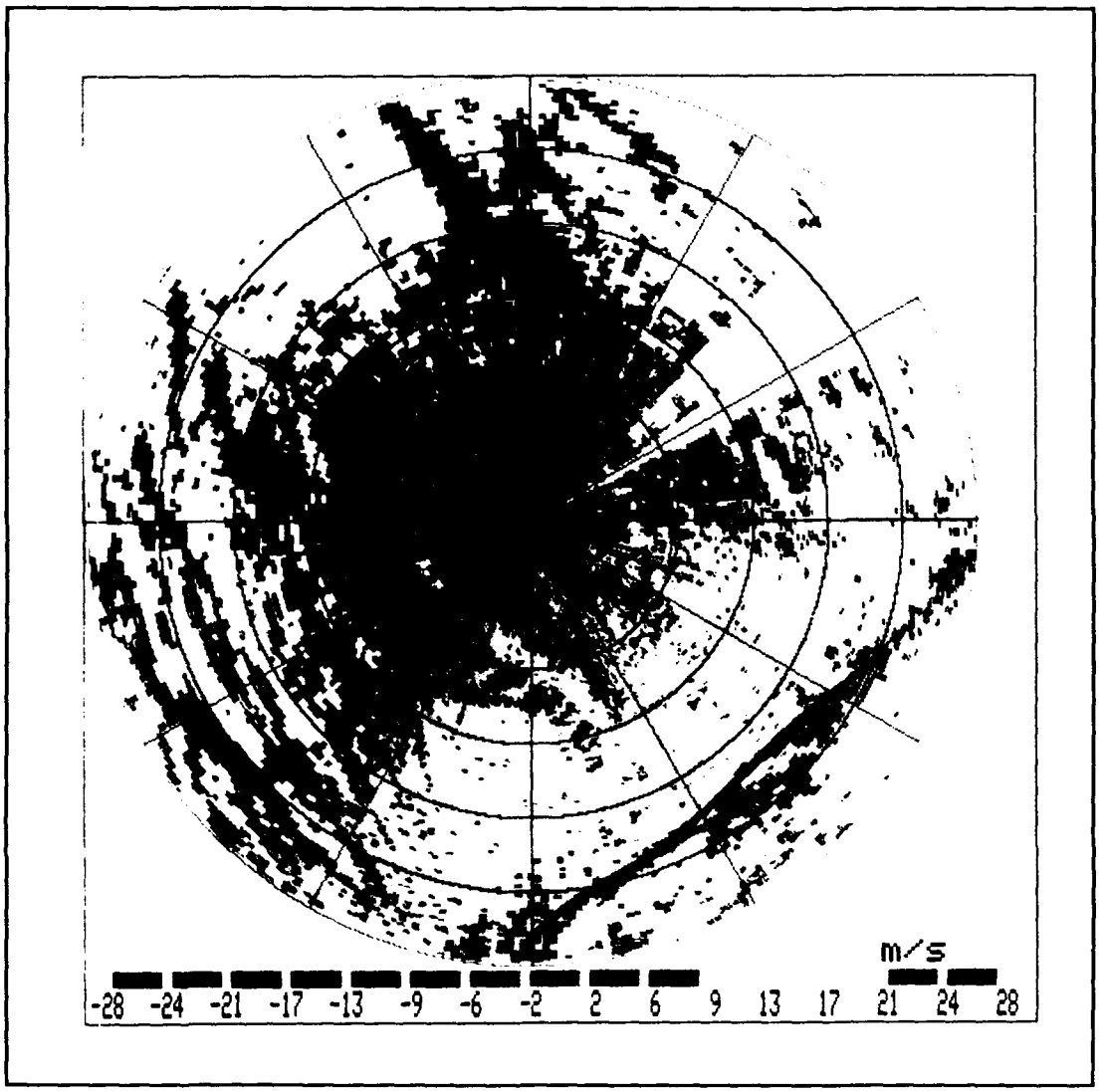

Fig. 3. Same as Fig. 2 except for the 0.5° tilt at 2155 UTC 24 March 1988. Gust front detection is in black.

5.2 Gravity waves.

Christie and Muirhead (1983) define gravity waves as "large amplitude single-created waves of elevation which propagate in waveguides formed by inversions in the lower atmosphere". They are produced by a wide variety of phenomena including

intense thunderstorms. They can occur in clear air, or can be accompanied by roll cloud(s) or "morning glories" (Smith, 1988). The wind shears associated with these phenomena may be very dangerous to aircraft, especially when the waves are not accompanied by a roll cloud and are invisible (Christie and Muirhead, 1983).

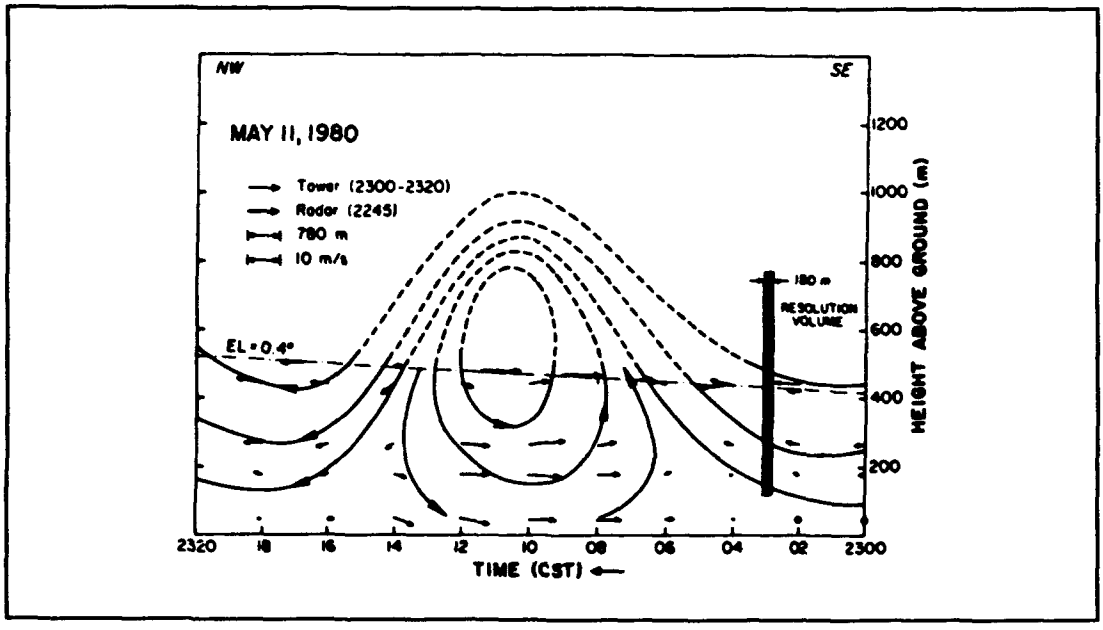

Fig. 4. Samples of winds (lightly traced arrows) measured at four tower levels along a NW-SE cross section corresponding to a Norman Doppler radar beam for the period 2300-2320 UTC 11 May 1980. The velocity scale is in the upper left corner. Bold arrows are Doppler radar estimates of wind at 2245 UTC projected onto the cross-section. The dashed streamlines are subjectively estimated in the data void region between 500 and 1000 m. From Doviak and Ge (1984).

Figure 4 presents observations from an instrumented tower and Doppler-radar radial velocity estimates of a single gravity wave (solitary wave) observed in Central Oklahoma on 11 May 1980 (Doviak and Ge, 1984). This particular wave was launched by a thunderstorm outflow onto an inversion layer formed by the passage of an earlier storm. The gravity-wave wind field is composed of a narrow band of negative (inbound) radial velocities. The environmental wind on either side of the

wave was moving radially outbound from the radar with equal speeds on both sides of the wave.

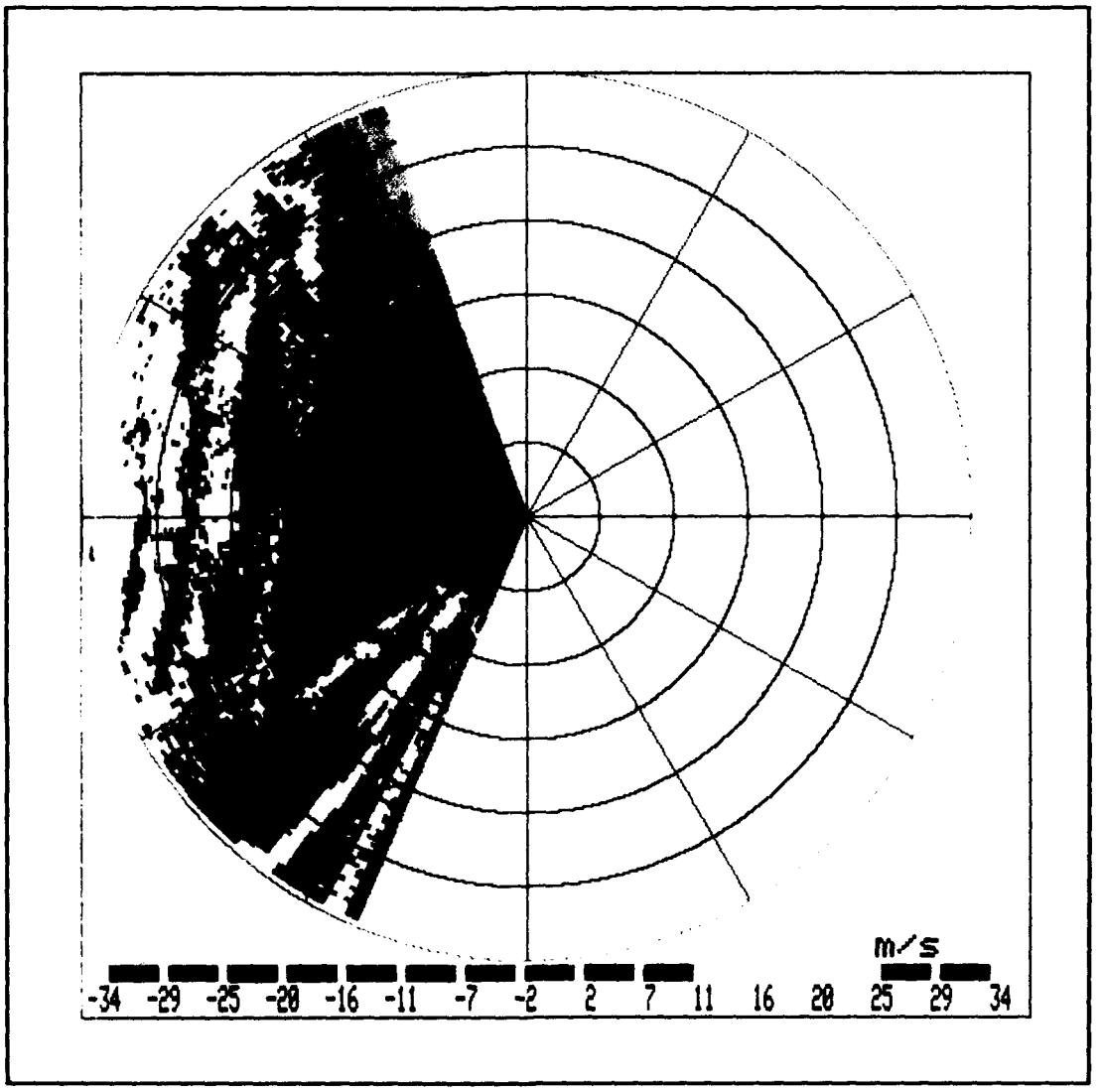

Fig. 5. Same as Fig. 2 except for the 0.5° tilt at 1612 UTC 22 June 1987. Gust front detections are in black.

The algorithm was tested on a Central Oklahoma case that consisted of not one, but several gravity waves moving toward the Norman Doppler radar on 22 June 1987. These data were collected using a high gain mode providing for better sensitivity of clear air returns. As many as 5 separate waves were observed within 60

km of the radar site (with up to 11 found within 120 km of the radar). These waves appeared on the radar as parallel bands of reflectivity at 1612 UTC (Fig. 5). The leading edges consisted of a band of outbound velocities, and the trailing edge of the two closest waves consisted of bands of inbound velocities. On radar, convergence was found along the leading edges of the waves. The GFDA produced two detections along the two closest waves at 1612 UTC.

As time went on, and as the waves approached the radar, the GFDA ceased producing detections. Shear features were still detected at the upper tilts. At the lower tilts, convergence in the velocity field was no longer measured (all velocities were inbound). Several factors might have accounted for this. First, the waves could have been losing their energy, and as a result, the radial convergence was weakening. Second, the waves may have been travelling along an inversion layer above the ground. As they approached the radar, the lower-elevation radar beam (0.5° tilt angle) may have undercut the strong convergence (shear features disappeared from the lower tilts first).

In order for the GFDA to detect radial shear segments, convergence must occur across a minimum radial distance (or peak shear "window"). This minimum distance is a factor of sample volume spacing (Stumpf, 1991). Detectability of gravity wave groups will suffer if the distance between successive waves is less than this minimum distance.

5.3 Sea and land breeze fronts.

Differential heating between land and water forces mesoscale circulations commonly found along shorelines of the oceans and large lakes (Atkinson, 1981). During the day, a sea (or lake) breeze consisting of cool humid air will blow onshore at low levels. Aloft, a return flow blows offshore. The situation is reversed during a land breeze. The land breeze is typically weaker than a sea-breeze (Lambert, 1974), and measurements of the land breeze fronts are rare since they usually occur over water.

Fronts are found at the leading edges of sea and land breezes. These fronts delineate opposing cool and warm air masses. As these sea (land) breeze fronts move onshore (offshore), the convergence associated with them can initiate convection. The wind shifts associated with these fronts will impact runway operations. It is unknown whether there has been an aircraft accident involving a sea breeze front.

Reported characteristics of the sea-breeze front vary in the literature. According to Atkinson (1981), the average speed is about 2 to 8 m s^{-1}. The depth of the onshore flow is about 150 to 2000 meters with the strongest onshore winds being measured about 250 m above the surface. Sea-breeze fronts penetrate inland anywhere from a few kilometers to sometimes over 300 km. Figure 6 shows a cross section through a typical sea breeze from Simpson, et al. (1977). Here, the front is about 600 m deep at its leading edge, and the convergence is measured across about

a 1 to 2 km horizontal distance. The depth of a typical sea-breeze is about equal to, or slightly shallower than a typical gust front.

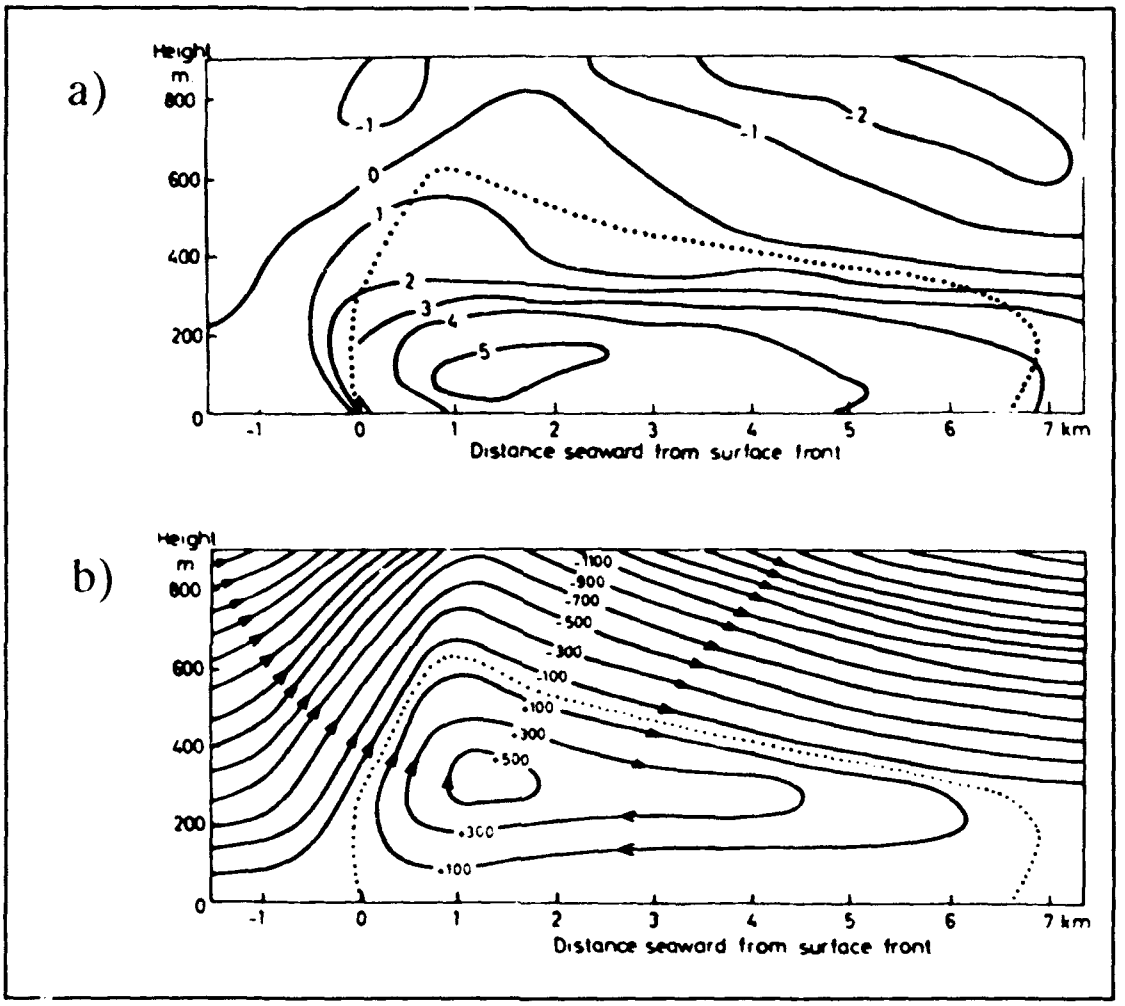

Fig. 6. (a) Vertical cross-section across a sea-breeze front showing southerly (cross-front) wind component of the wind field at 1700-1800 UTC 14 June 1973. Isopleths are in m s^{-1}. Dotted line shows interface of sea breeze front; (b) Streamlines of flow relative to sea-breeze front. Contour interval is 100 m^3 s^{-1} per meter thickness. The zero streamline (dotted) marks the front boundary. From Simpson et al. (1977).

Some sea and lake breeze fronts should be detectable by the GFDA. Lyons (1972) measured convergence of 3 x 10^{-3} s^{-1} across a 1-2 km wide lake breeze front

case. From Eq. (1), this corresponds to a horizontal wind shear of 1.5 m s^{-1} km^{-1} which is just below the typical threshold setting of 2 m s^{-1} km^{-1}. From the example shown in Fig. 6, velocity differences of up to 5 m s^{-1} are measured across a 1 km distance about 100 m above the ground. This is within the typical algorithm threshold for velocity difference. Stronger fronts can occur (up 8 m s^{-1} speeds behind them). In fact, Kraus *et al.* (1990) measured velocity differences across sea-breeze fronts in Australia to be as high as 14 m s^{-1}. Convergence along sea-breeze fronts will be higher when the fronts oppose strong synoptic flow.

Detecting shallow or distant gust fronts presents a problem (Stumpf, 1991). When the radar beam no longer intersects the shear zone associated with a shallow or distant gust front, is may go undetected. In a sea breeze situation, a return offshore flow is found in the layer above the onshore flow. At higher radar beam heights, the sea-breeze circulation may actually be seen as a divergent pattern rather than a convergent pattern. In these situations, the GFDA would not be able to detect the sea-breeze front.

During the summers of 1990 through 1992, Doppler radar data were collected during a TDWR field experiment in Orlando FL using the Massachusetts Institute of Technology's Lincoln Laboratory FL-2 testbed radar. The radar site was located some 50-60 km from the Atlantic Ocean, and there was an opportunity to collect data sets containing sea-breeze fronts. The GFDA was tested on one such case from 10 August 1991. Figure 7 shows that this sea breeze was detected as a 25 km long gust front with an average across-front velocity difference of nearly 10 m s^{-1}. The sea breeze was detected on 7 consecutive scans (a 35-minute period).

Fig. 7. Radial velocity field for the 0.5° tilt at 1955 UTC 10 August 1990 from the Massachusetts Institute of Technology/Lincoln Laboratory (MIT/LL) FL-2 Doppler radar near Orlando, Florida. Range rings are every 10 km. Gust front detection is in red.

5.4 Other radar-observed boundary layer-convergence lines.

Wilson and Schreiber (1986) have shown that a variety of organized lines of convergence in the boundary layer besides gust fronts, synoptic fronts, and sea-breeze

fronts, can be responsible for the initiation of convective storms. Some of these convergence lines have been linked to orographically-induced circulations such as the Denver Convergence Vorticity Zone (DCVZ; Fig. 8; Szoke *et al.*, 1984) or "mountain outflows" (Schlatter *et al.*, 1985). Others have been linked to circulations forced by differential heating of different land types (i.e., vegetation differences, soil color differences, cloud cover, snow cover, etc.; Pielke and Segal, 1986). Also, some convergence lines are the result of "old" gust fronts or outflows from larger mesoscale convective systems (MCSs) which have become quasi-stationary over a 2-12 hour time scale (Fig. 9; Purdom, 1982).

Knowledge of the location of these lines to NWS forecasters is of importance to mesoscale convective forecasting, especially when convergence lines collide with other lines or with old thunderstorms (Wilson and Schreiber, 1986). In a similar instance, Roberts and Wilson (1989) show a DCVZ case where a terrain induced boundary dissipated (presumably because the synoptic flow field over the terrain weakened). However, this former boundary left behind a zone of moisture that was favorable for rapid storm development which initiated when gust fronts from nearby convection collided within this moisture zone.

Since these convergence lines are lesser known to a degree than gust fronts, their characteristics cannot be easily compared to those of gust fronts. Wilson and Schreiber (1986) have found, however, that these phenomena are observed with similar horizontal space scales as gust fronts in northeast Colorado, but their strength and vertical space scales are not as well understood.

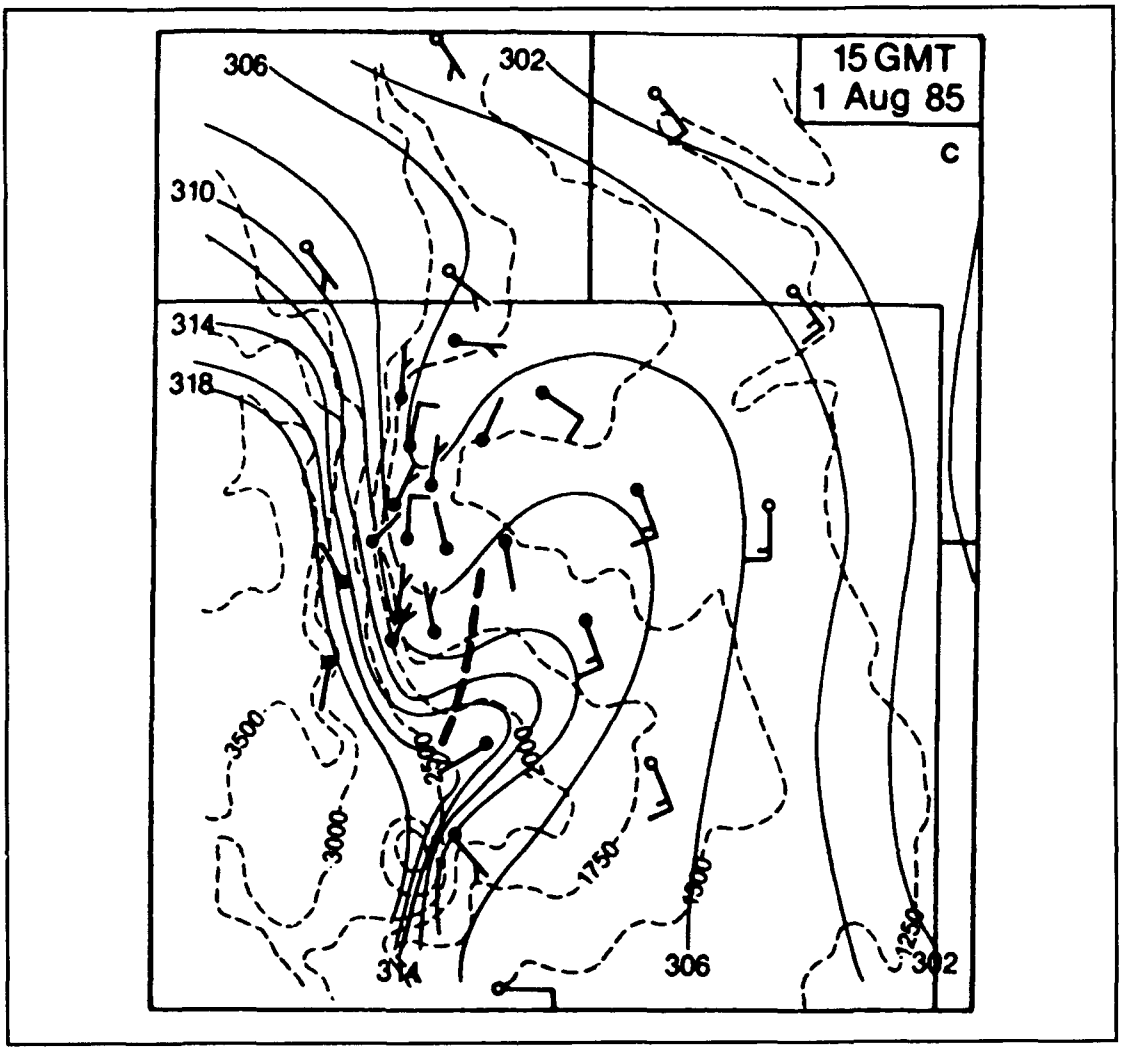

Fig. 8. Surface observations of wind and potential temperature at 1500 UTC 1 August 1985 in Northeast Colorado. Potential temperature (solid lines) contour interval is 2K; selected terrain contours are shown with thin dashed lines. The DCVZ is shown with a heavy dashed line. From Wilczak and Glendening (1988).

The GFDA was tested on data from a DCVZ case in northeast Colorado during 5 June 1988. On this day, a mesoscale convergent area was observed in a local surface mesonetwork of automated instrumented stations. Strong convection developed along this zone. The algorithm was tested on radar data collected before and during convective initiation.

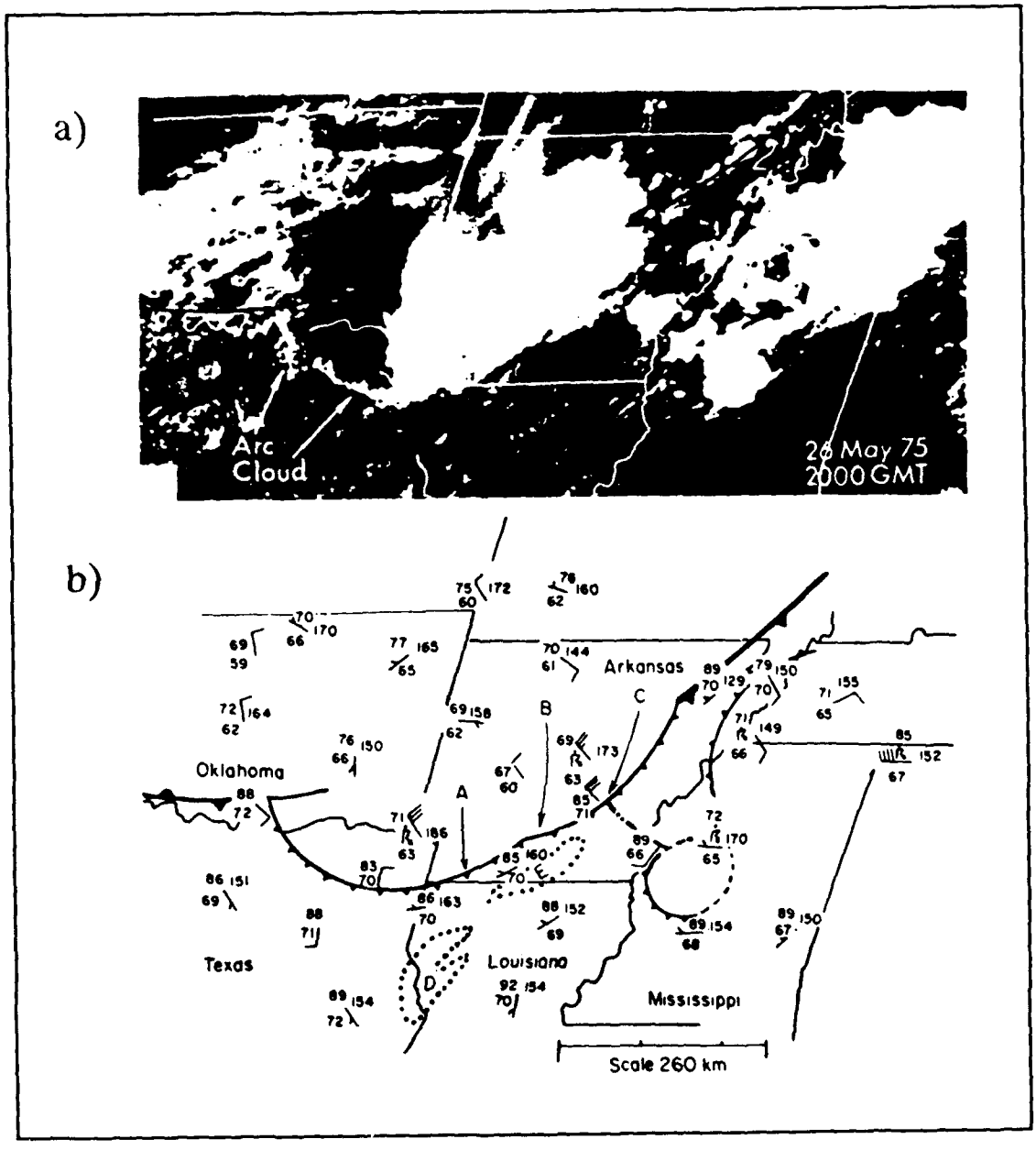

Fig. 9. Visible satellite picture and horizontal surface mesoanalysis of thunderstorm outflow boundaries at 2000 UTC 26 May 1975. Outflow boundaries are represented using cold front symbols except with smaller "spikes". From Purdom (1982).

Before the convection developed, the algorithm produced no front detections. Several factors accounted for this. Signal strength on the west side of the boundary was weak (where signal to noise ratios were below the 0 db algorithm threshold).

Also, convergence occurred over a broad area (5-15 km) instead of being concentrated as in a typical gust front (1-3 km). Peak shear values were below algorithm threshold settings.

At 2027 UTC on the 0.5° tilt (Fig. 10a), the boundary was located 30-50 km northwest of the radar. Only one 10 km feature on the 0.5° tilt was detected. This was where the boundary lay most perpendicular to radials and the maximum radial convergence could be measured. On the 1.0° tilt (Fig. 10b), almost no signal was returned on the northwest side of the boundary. Only after convection developed along the terrain-induced boundary were detections produced by the algorithm. These detections were the result of actual gust fronts produced by thunderstorm downdrafts.

The GFDA was also tested on an Oklahoma case on 15 June 1987 where an area of boundary-layer convergence lines were observed on radar in a basically precipitation free area that stretched southwest through west-northwest of the Norman radar at ranges between 30 and 60 km. No converging velocities were observed at 2133 UTC (Fig. 11), but weak thin lines were evident in the reflectivity pattern. Shear features are not detected until later when a gust front, created by dissipating storms about 90 km southwest of the radar, moved in and intersected these boundaries. Weak convergence first becomes visible at this time, but only small shear features and no front detections were produced by the algorithm. Convection later developed along these intersecting boundaries.

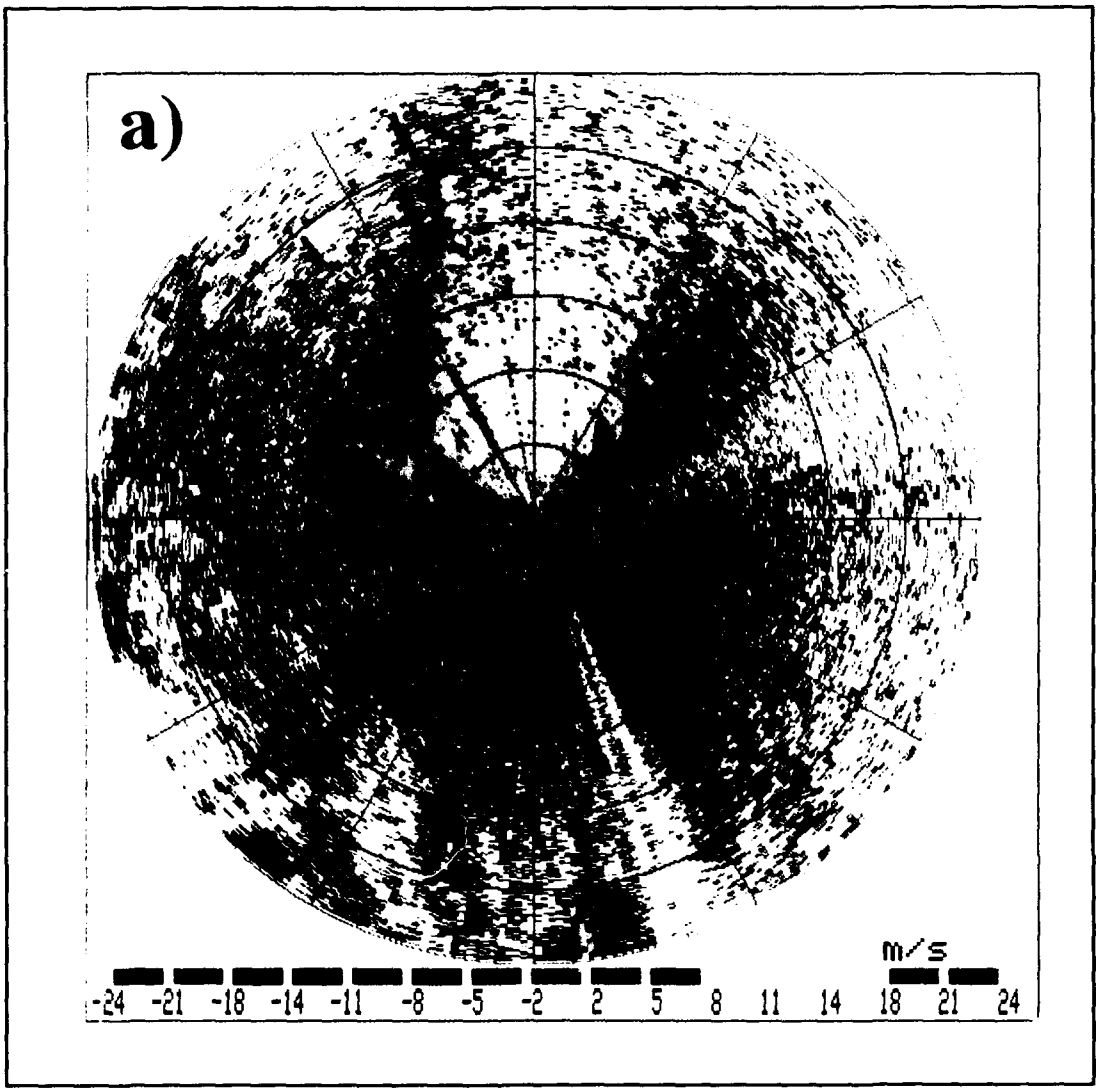

Fig. 10. *Radial velocity field at 2027 UTC 5 June 1988 from the Massachusetts Institute of Technology/Lincoln Laboratory (MIT/LL) FL-2 Doppler radar near Denver, Colorado; a) 0.5° tilt; b) 1.0° tilt. Range rings are every 10 km. Positive (negative) velocity values (m s^{-1}) represent velocities away (toward) the radar.*

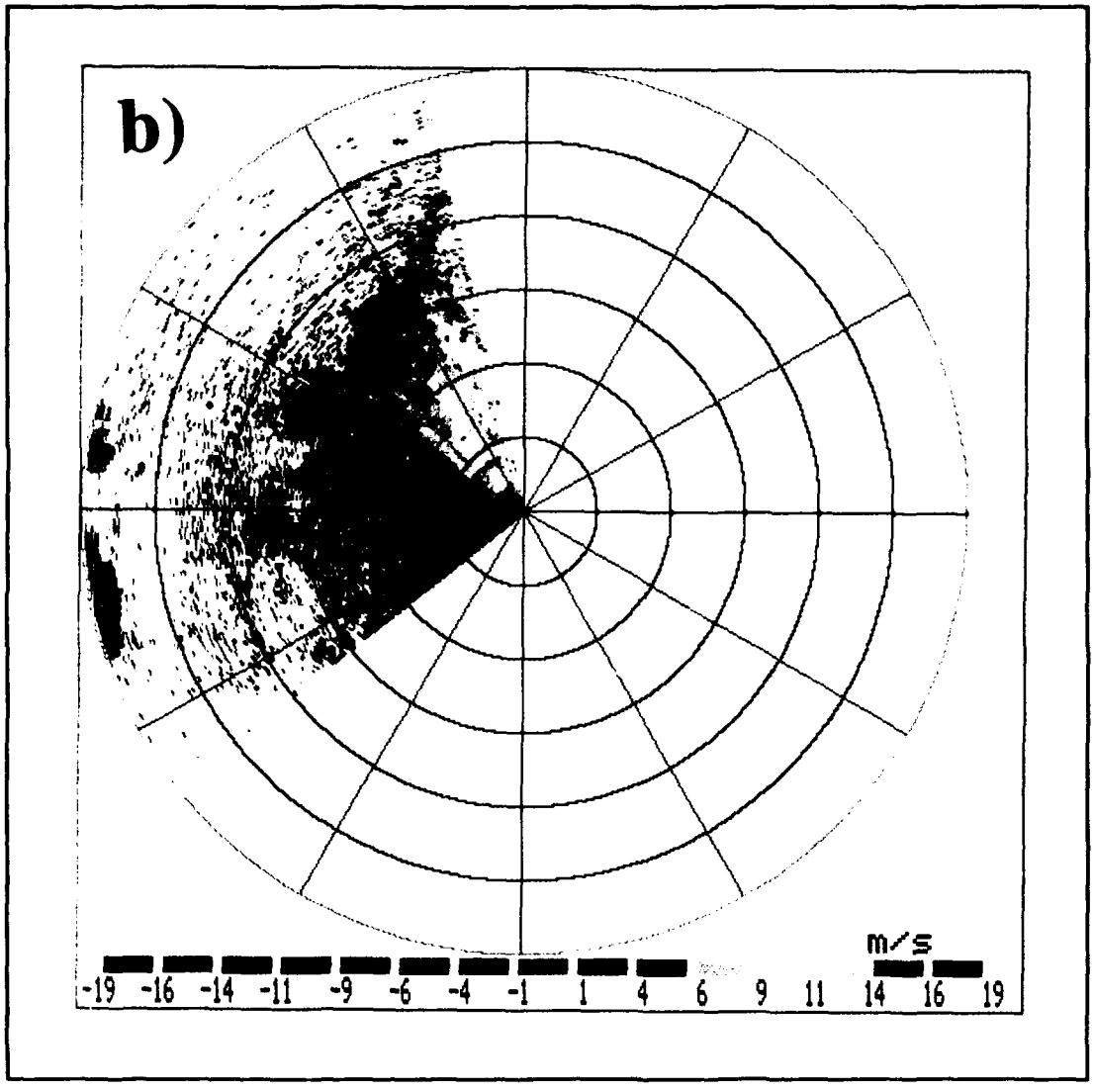

Fig. 10. *(continued)*

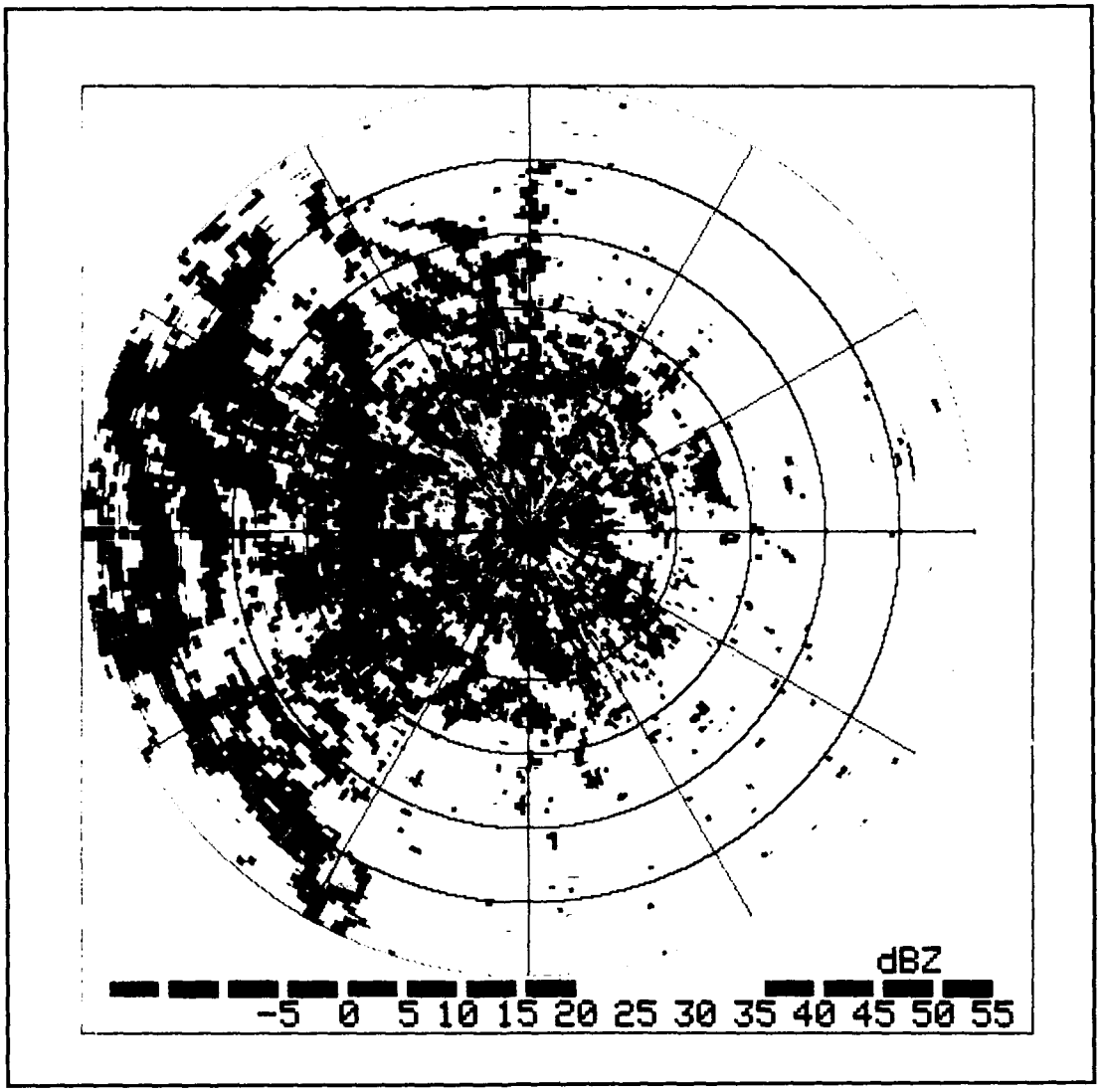

Fig. 11. *Reflectivity field (dBz) for the 0.5° tilt at 2133 UTC 15 June 1987 from the NSSL Norman, Oklahoma Doppler radar. Range rings are every 10 km.*

5.5 Precipitation bands in extratropical cyclones.

In extratropical storms, bands of enhanced precipitation are commonly observed and they can vary in width, depth, length, strength, and location within a synoptic-scale storm (Houze, et al., 1976). Rain and snow bands, for instance, are commonly found on the cold air side of warm fronts (Heymsfield, 1979; Sanders and Bosart, 1985; Wolfsberg et al., 1986). These bands of precipitation are hypothesized to be caused by convergence. Detecting these bands by the GFDA may aid in predicting mesoscale precipitation amounts and coverage area. Ramamurthy *et al.* (1991) showed that on some occasions, precipitation bands observed during winter storms during a field project in Illinois produced localized heavy amounts of snow, damaging glaze (freezing rain), and lightning.

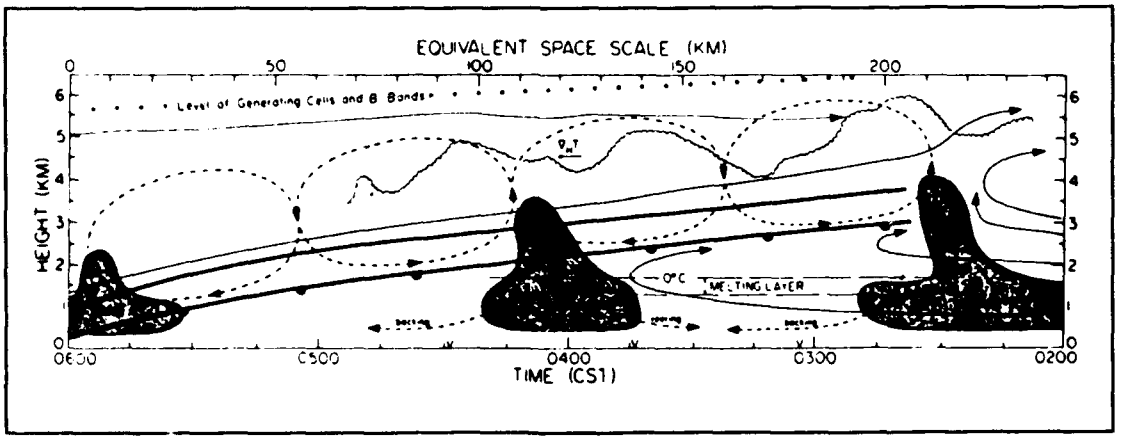

Fig. 12. *Schematic of warm front structure derived from a Doppler radar time-height cross-section on 26 March 1976. Thick lines enclose warm frontal zone. Streamlines are shown for large-scale front relative flow (solid lines), and secondary circulations relative to front (dashed lines). Radar cloud tops (scalloping) and time of vertical incidence observations are shown. From Heymsfield (1979).*

In each of the three warm front studies (Heymsfield, 1979; Sanders and Bosart, 1985; Wolfsberg et al., 1986), Doppler radar confirmed the existence of rolls in the airflow associated with the bands. Figure 12 shows a vertical cross-section schematic of the warm front rain bands observed by Heymsfield (1979). In his schematic, the bands coincided with convergence at and just above the frontal surface about 1-4 km above the ground. He measured convergence at a 3.3 km altitude of about 6 x 10^{-4} s^{-1} across about a 3-5 km width (Fig. 13).

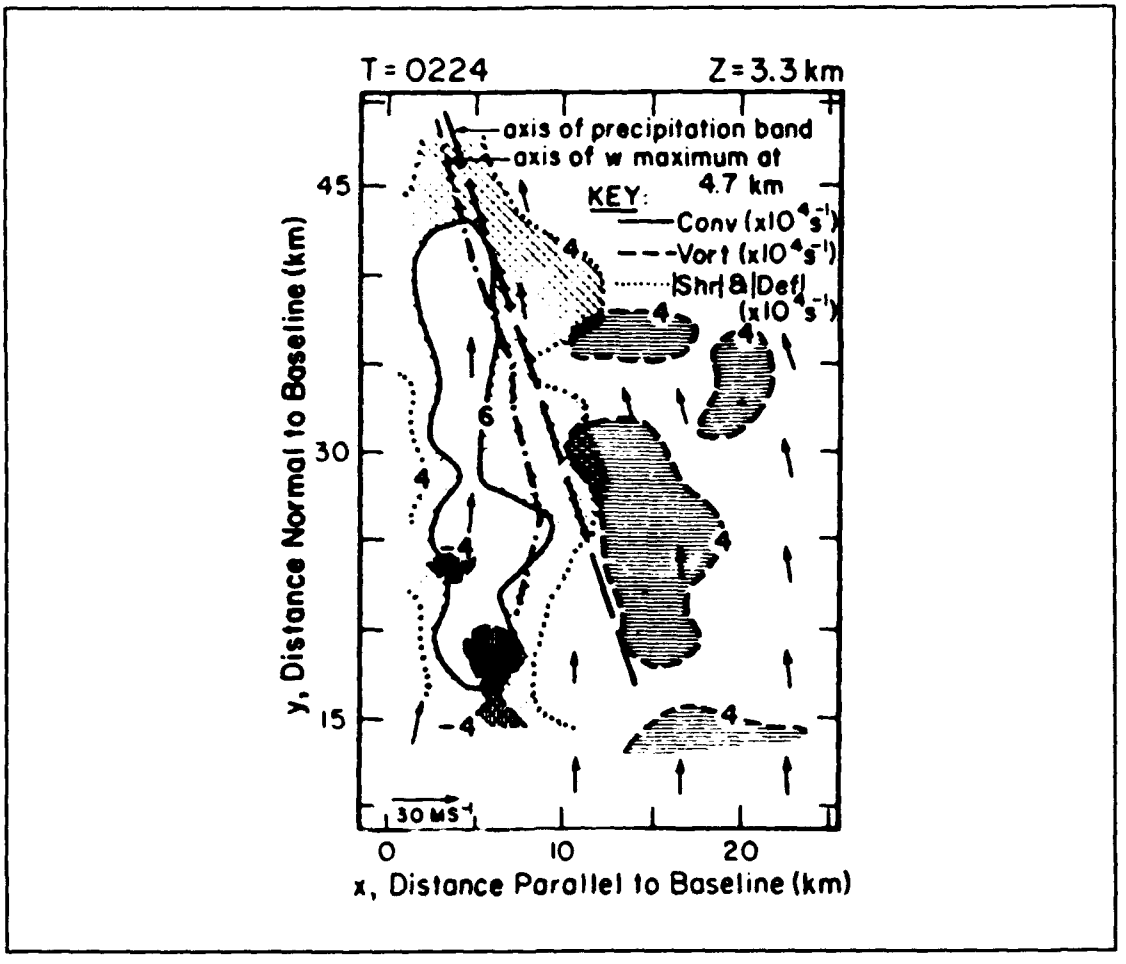

Fig. 13. *Horizontal analysis of one warm front band from Fig. 12. Arrows represent winds relative to band motion.*

For the case in Fig. 13, velocity differences are computed to be about 0.9 to 1.5 m s^{-1} across a 3 to 5 km distance. The horizontal wind shear is about 0.3 m s^{-1} km^{-1}. The typical algorithm threshold setting for peak shear across radial shear segments is 2 m s^{-1} km^{-1}. The computed velocity differences in Heymsfield's case are much lower than the minimums specified by the threshold settings. Therefore, if these values are typical for warm frontal precipitation bands, they will not be detected.

Below the melting layer, the bands were associated with divergence (Fig. 12) with the convergence being observed between the bands instead of along them. This divergence was postulated to be produced by pressure perturbations created by the melting of ice particles. When precipitation consists of snow instead of rain, the low-altitude divergence is normally not present. If a melting layer exists, and if liquid (as opposed to frozen) precipitation is reaching the ground, and if the radar beams are below the melting layer, the GFDA would detect convergence between the bands instead of along them.

Since these bands normally consist of narrow lines of enhanced reflectivity, a reflectivity thin line algorithm similar to the one used in the AGFDA (Eilts *et al.*, 1991), or a modification to that algorithm, could be used to detect these phenomena.

6. Conclusion.

In summary, we have shown that a variety of weather phenomena can be detected by the Gust Front Detection Algorithm. The GFDA was tested on a

number of cases of actual radar data, and the algorithm successfully identified a non-precipitating synoptic cold front, a series of boundary-layer gravity waves, a sea-breeze front, and a convergence line induced by an orographic circulation.

In general, if a weather phenomenon has the radar-observed convergence characteristics similar to a gust front, the GFDA can detect them. The phenomenon must be associated with a convergent wind field of a sufficient strength (an average velocity difference of 7 m s^{-1} or greater and an average shear of 2 m s^{-1} km^{-1}), depth (must be detectable on both a 0.5° and 1.0° tilt), and length (at least 10 km), to pass the algorithm thresholds for detection.

However, some of these phenomena were still too weak to be detected with the GFDA. The site adaptable convergence strength thresholds could be lowered to enhance detectability of the weaker cases. By lowering the thresholds used for convergent shear segment building, more "noise" can get passed through the algorithm, and a greater amount of false alarms might be detected.

Many of these non-gust front phenomena are not associated with significant precipitation and occur in "clear-air" (e.g., non-precipitating synoptic cold fronts). Signal-to-noise ratios (SNR) are typically lower in clear air. If the SNR of a Doppler-radar radial velocity estimate is below the site-adaptable threshold of 0 dB, the GFDA will consider it an unusable velocity. If a clear-air operating mode were used, SNRs would increase. For example, an operating mode similar to the WSR-88D scan strategy 3 long pulse width mode could be used to gain detections at these weak noise levels. This WSR-88D clear-air mode has an increased sensitivity of about 8 dB over the WSR-88D precipitation mode (Heiss et al., 1990). However, sample

volume resolution is about 6 times that of the TDWR system, and the GFDA detection capability becomes degraded (Stumpf, 1991).

Furthermore, reflectivity thin lines were observed for many of these cases, including the ones with associated weak convergence. Moisture is typically concentrated in these zones and refractivity index gradients enhances the reflectivity field. An advanced version of the GFDA is currently being developed which will have the capability to detect reflectivity thin lines (Eilts *et al.*, 1991).

These case studies represent a limited data base with which to test the GFDA. For each type of phenomena, there are a multitude of situations which could lead to varied results. Most of the data were collected at different locations using different radars with different tilt strategies. In order to complete a more comprehensive study, an effort needs to made to collect data sets containing different examples of these phenomena. Fortunately, with the deployment of the WSR-88D network nationwide, and its capability to archive radar data efficiently (T. Crum, personal communication), the potential exists in the next decade to amass an extensive library of data comprising these weather phenomena. This will result in a better understanding of the structure and evolution of these phenomena so that they are more easily identifiable by radar-based weather algorithms.

7. References.

Atkinson, B. W., 1981: *Meso-scale Atmospheric Circulations.* New York, Academic Press, 495 pp.

Brandes, E. A., and R. M. Rabin, 1991: Probing a nonprecipitating cold front with Doppler weather radar. *J. Atmos. and Oceanic Tech.*, **8**, 409-421.

Browning, K. A., 1971: Radar measurements of air motion near fronts. *Weather*, **26**, 320-340.

Christie, D. R., and K. J. Muirhead, 1983: Solitary waves: a low-level wind shear hazard to aviation. *Int. J. Aviation Safety*, 169-190.

Doviak, R. J., and R. Ge, 1984: An atmospheric solitary gust observed with a Doppler radar, a tall tower and a surface network. *J. Atmos. Sci.* **41**, 2559-2573.

Doviak, R. J., and D. S. Zrnić, 1984: *Doppler Radar and Weather Observations.* Orlando, Academic Press. 458 pp.

Eilts, M. D., S. H. Olson, G. J. Stumpf, L. G. Hermes, A. Abrevaya, J. Culbert, K. W. Thomas, K. Hondl, and D. Klingle-Wilson, 1991: An improved gust front detection algorithm for the TDWR. *Preprints, 25th Conf. on Radar Meteor.*, Paris, France, June 24-28, Amer. Meteor. Soc., J37-J42.

Heiss, W. H., D. L. McGrew, and D. Sirmans, 1990: Nexrad: Next generation weather radar (WSR-88D). *Microwave Journal*, **33**, 79-98.

Hermes, L. G., K. W. Thomas, G. S. Stumpf, and M. D. Eilts, 1990: Enhancements to the TDWR Gust Front Algorithm. Federal Aviation Administration Report No. DOT/FAA/NR-91/3, 55 pp.

Heymsfield, G. M., 1979: Doppler radar study of a warm frontal region. *J. Atmos. Sci.*, **36**, 2093-2107.

Houze, R. A., P. V. Hobbs, K. Biswas, W. M. Davis, 1976: Mesoscale rain bands in extratropical cyclones. *Mon. Wea. Rev.*, **104**, 868-878.

Klingle, D. L., D. R. Smith, and M. M. Wolfson, 1987: Gust front characteristics as detected by Doppler radar. *Mon. Wea. Rev.*, **115**, 905-918.

Kraus, H., J. M. Hacker, and J. Hartmann, 1990: An observational aircraft-based study of sea-breeze frontogenesis. *Bound.-Layer Meteor.*, **53**, 223-265.

Lambert, S., 1974: High resolution numerical study of the sea-breeze front. *Atmosphere*, **12**, 97-105.

Lyons, W. A., 1972: The climatology and prediction of the Chicago lake breeze. *J. Appl. Meteor.*, **11**, 1259-1270.

Maddox, R. A., L. R. Hoxit, and C. F. Chappell, 1980: A study of tornadic thunderstorm interactions with thermal boundaries. *Mon. Wea. Rev.*, **108**, 322-336.

Parsons, D. B., 1991: Radar observations and numerical simulations of the mesoscale structure of surface cold fronts. *Preprints, 25th Int'l. Conf. on Radar Meteor.*, Paris, France, June 24-28, Amer. Meteor. Soc., 164-168.

Pielke, R. A., and M. Segal, 1986: Mesoscale circulations forced by differential heating. In: *Mesoscale Meteorology and Forecasting*, Ray, P., Ed., Amer. Meteor. Soc., 516-548.

Purdom, J. F. W., 1982: Subjective interpretations of geostationary satellite data for nowcasting. *Nowcasting*, K. Browning, Ed., Academic Press, 149-166.

Ramamurthy, M. K., R. M. Rauber, B. P. Collins, M. T. Shields, P. C. Kennedy, and W. L. Clark, 1991: UNIWIPP: A University of Illinois field experiment to investigate the structure of mesoscale precipitation in winter storms. *Bull. Amer. Meteor. Soc.*, **72**, 764-776.

Roberts, R. D., and J. W. Wilson, 1989: Multiple Doppler radar analysis of the 15 June 1988 Denver tornado. *Preprints, 24th Conf. on Radar Meteor.*, Tallahassee, FL, Amer. Meteor. Soc., 142-145.

Sanders, F., and L. F. Bosart, 1985: Mesoscale structure in the megalopolitan snowstorm, 11-12 February 1983. Part II: Doppler radar study of the New England snowband. *J. Atmos. Sci.*, **43**, 1398-1407.

Schlatter, T. W., P. Schultz, and J. M. Brown, 1985: Forecasting convection with the PROFS system: Comments on the summer of 1983 experiment. *Bull. Amer. Meteor. Soc.*, **66**, 802-809.

Simpson, J. E., D. A. Mansfield, and J. R. Milford, 1977: Inland penetration of sea-breeze fronts. *Quart. J. Royal Meteor. Soc.*, **103**, 47-76.

Smith, R. K., 1988: Travelling waves and bores in the lower atmosphere: the 'morning glory' and related phenomena. *Earth-Sci. Rev.*, **25**, 267-290.

Stumpf, G. S., 1991: On the potential use of the Terminal Doppler Weather Radar Gust Front Detection Algorithm on the WSR-88D system, Part I: Impacts of radar system differences. Submitted as an Federal Aviation Administration Report.

Szoke, E. J., M. L. Weisman, J. M. Brown, F. Caracena, and T. W. Schlatter, 1984: A subsynoptic analysis of the Denver tornadoes of 3 June 1981. *Mon. Wea. Rev.*, **112**, 790-808.

Uyeda, H., and D. S. Zrnić, 1985: Automatic detection of gust fronts. Federal Aviation Administration Report No. DOT/FAA/PM-85/11, 51 pp.

Wilczak, J. M., and J. W. Glendening, 1979: Observations and mixed-layer modeling of a terrain-induced mesoscale gyre: The Denver Cyclone. *Mon. Wea. Rev.*, **116**, 2688-2711.

Wilson, J. W., and W. E. Schreiber, 1986: Initiation of convective storms at radar-observed boundary layer convergence lines. *Mon. Wea. Rev.*, **114**, 2516-2536.

Witt A., and S. D. Smith, 1987: Development and testing of the gust front algorithm. Federal Aviation Administration Report No. DOT/FAA/PS-87/4, 30 pp.

Witt, A., S. D. Smith, M. D. Eilts, L. G. Hermes, and D. L. Klingle-Wilson, 1989: Gust front/wind shift detection algorithm for the Terminal Doppler Weather Radar. Federal Aviation Administration Report No. DOT/FAA/NR-91/4, 64 pp.

Wolfsberg, D. G., K. A. Emanuel, and R. E. Passarelli, 1986: Band formation in a New England winter storm. *Mon. Wea. Rev.*, **114**, 1552-1569.